

THE MAGNETAR XTE J1810–197: VARIATIONS IN TORQUE, RADIO FLUX DENSITY AND PULSE PROFILE MORPHOLOGY

F. CAMILO,¹ I. COGNARD,² S. M. RANSOM,³ J. P. HALPERN,¹ J. REYNOLDS,⁴ N. ZIMMERMAN,¹ E. V. GOTTHELF,¹ D. J. HELFAND,¹
P. DEMOREST,⁵ G. THEUREAU,² AND D. C. BACKER⁵

Submitted to The Astrophysical Journal, October 22, 2006

ABSTRACT

We report on observations of the radio-emitting anomalous X-ray pulsar XTE J1810–197 during 2006 May–October using the Nançay, Parkes, GBT, and VLA telescopes at a frequency of 1.4 GHz. The torque experienced by the neutron star during this period, as inferred from a measurement of its rotational frequency derivative, decreased by 30%, although not in a steady manner. We have also observed very large ongoing fluctuations in flux density and pulse shape. Superimposed on these, a general diminution of flux density and a broadening of the pulse profile components occurred nearly contemporaneously with a decrease in torque of about 10% that took place in late July over an interval of two weeks. In addition, a simultaneous observation of the pulsar with the *Chandra X-ray Observatory* and the GBT allows us to show how the X-ray and radio profiles are aligned. We discuss briefly the implications of these results for the magnetospheric currents in this remarkable object.

Subject headings: pulsars: individual (XTE J1810–197) — stars: neutron

1. INTRODUCTION

The transient anomalous X-ray pulsar (AXP) XTE J1810–197 ($P = 5.54$ s) was discovered in early 2003 when its X-ray luminosity increased ~ 100 -fold (Ibrahim et al. 2004) compared to the quiescent state maintained for > 24 years (Halpern & Gotthelf 2005). Initial X-ray observations revealed unsteady spin-down with $\dot{P} \approx 10^{-11}$ (implying a surface magnetic dipole field strength $B \approx 2 \times 10^{14}$ G) that varied by up to a factor of two within a few months of the outburst.

The origin of a radio source positionally coincident with the pulsar (Halpern et al. 2005) was clarified by the detection of strong, narrow, highly linearly polarized radio pulses once per stellar rotation (Camilo et al. 2006). This emission has several unique characteristics. First, it is at least one order of magnitude brighter than in the late 1990s, when it was undetected. Presumably the radio source turned on following the X-ray outburst. Just as the X-ray flux has now decayed to a level approximating the historical low state (Gotthelf & Halpern 2006), the radio emission can be expected to cease “shortly”. In the initial observations, Camilo et al. (2006) also noted that the radio flux density of XTE J1810–197 varied on time scales of approximately a day in a manner inconsistent with interstellar scintillation, implying large day-to-day radio luminosity changes not seen in ordinary pulsars. The “average” pulse profiles were also found to change in a manner seemingly inconsistent with variations observed in other neutron stars. Lastly, the magnetar has a very flat radio spectrum, and has been detected at higher radio frequencies than any other pulsar.

These unusual characteristics of XTE J1810–197 presum-

ably reflect different physical conditions in its magnetosphere compared both with those of ordinary radio pulsars and of persistent magnetars, which so far have shown no evidence of magnetospheric radio activity. The study of this radio emission thus provides a new window into the coronae of magnetars. We summarize here some results from our monitoring program for XTE J1810–197, focusing on rotational, flux density, and pulse profile evolution.

2. DATA ACQUISITION, ANALYSIS, AND RESULTS

2.1. Observations

2.1.1. Nançay

We have observed XTE J1810–197 at Nançay on most days since 2006 June 1 (MJD 53887) with typical integration times of 15–60 min, using the Berkeley-Orleans-Nançay (BON) coherent dedispersor (Cognard & Theureau 2006) based on a Serendip V spectrometer⁶. The Nançay radio telescope has a gain of 1.5 K Jy^{-1} and a system temperature of 47 K at 1.4 GHz in the direction of XTE J1810–197, which this meridian-type telescope can track for 1 hr each day. Dedispersion of a 64 MHz band centered on 1398 MHz is done coherently into 16 4 MHz channels using a 64-node computer cluster, with each data stream then folded every 2 min at the pulsar’s predicted period. In Figure 1 we show the daily folded pulse profiles obtained in the linear horizontal polarization (with dipole orientation parallel to the ground) after excising significant levels of radio frequency interference (RFI). Regional telephone relay and radio transmitters use the vertical polarization, leading to much more severe RFI in that channel. However, the radio emission from XTE J1810–197 is highly polarized and fortuitously is much stronger in the direction parallel to the ground at Nançay, so that the vertical signal is in any case usually very small (the parallactic angle change during the maximum integration is a negligible $\pm 2^\circ$).

Since July we have used a second observing system in parallel with BON, where square-law detectors sampled every 2 ms record the total power for each polarization channel in

¹ Columbia Astrophysics Laboratory, Columbia University, 550 West 120th Street, New York, NY 10027.

² Laboratoire de Physique et Chimie de l’Environnement, CNRS, 3A Avenue de la Recherche Scientifique, F-45071 Orleans, Cedex 2, France.

³ National Radio Astronomy Observatory, 520 Edgemont Road, Charlottesville, VA 22903.

⁴ Australia Telescope National Facility, CSIRO, Parkes Observatory, PO Box 276, Parkes, NSW 2870, Australia.

⁵ Department of Astronomy, University of California, Berkeley, CA 94720-3411.

⁶ See <http://seti.berkeley.edu/casper/projects/SERENDIP5/>

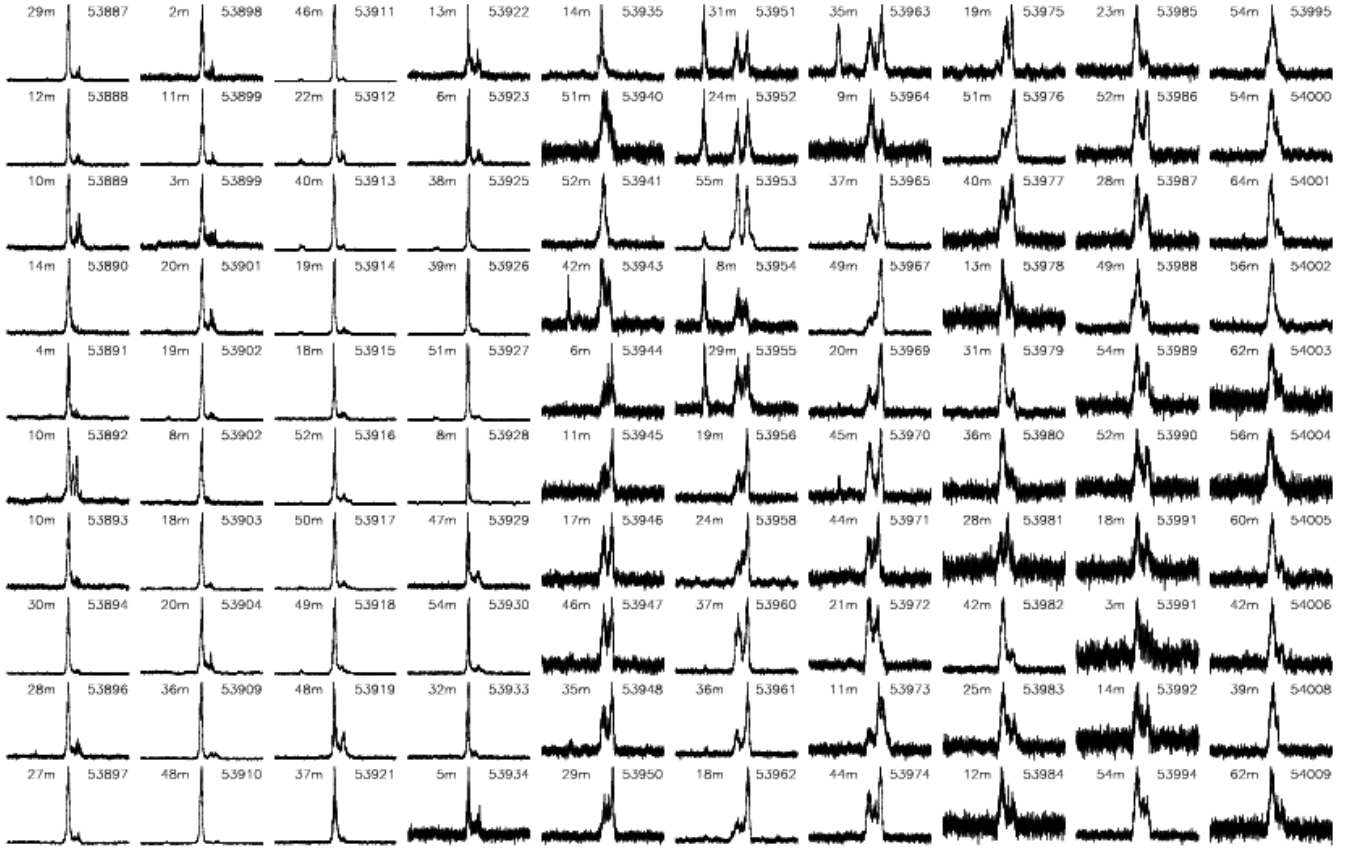


FIG. 1.— Daily pulse profiles from XTE J1810–197 recorded in the linear horizontal polarization at Nançay at a frequency of 1.4 GHz across a bandwidth of 64 MHz (§ 2.1.1), each displayed with 2048 bins (the first is from 2006 June 1 and the last from October 1). We aligned these profiles using an ephemeris containing seven frequency derivatives that resulted in featureless residuals (see § 2.2). Each profile is labeled with the effective integration time in minutes to its left (i.e., after the removal of RFI) and the observing date (MJD) to its right. In some cases minor artifacts remain, due to improperly excised RFI.

a 50 MHz band centered on 1410 MHz. These data are flux-calibrated by the firing of a calibrated pulsed noise diode at the beginning of each observation. However, this detector’s sampling rate is not stable enough for pulsar timing purposes, for which we use the accurately time-tagged BON records.

We have used data from both systems to obtain flux density estimates for the daily profiles. The square-law detected outputs suffer less from RFI (because of their higher central frequency and narrower bandwidth) and are accurately flux-calibrated. On the other hand, removal of RFI in these records is complicated by the lack of frequency resolution. For BON data we first carefully removed RFI in the time-frequency plane and then used the radiometer equation, along with the known telescope noise characteristics, to convert the rms noise fluctuation in the off-pulse part of the profiles to a Jansky scale. We determined this conversion factor for the horizontal polarization and applied it to both channels. We then added the corresponding profiles from both polarizations and, by integrating the area under each profile, finally measured the pulsed flux density. On most days the flux densities estimated from the two systems agree to within $\sim 25\%$, and hereafter we use only the BON values.

It is evident from Figure 1 that the pulse profiles are not stable, particularly after late July (MJD 53935 is July 19). This presents obvious difficulties for obtaining pulse times-of-arrival (TOAs) by following the usual prescription of cross-correlating a “standard profile” with each day’s profile. Instead, we obtain TOAs from the maximum of a parabola fitted to one pulse profile component that, we assume, regardless of

variations, corresponds to the same longitudinal fiducial point on the pulsar. We choose for this fiducial point the left-most of the (typically) two components that make up the main cluster of emission. This choice is motivated by the facts that, within our large and densely sampled set of observations, *i*) the longitudinal separation between the corresponding peaks ($0.08P$) remains essentially fixed even as the profiles vary enormously (e.g., see the profiles for MJDs 53919 and 53961 in Fig. 1, for which the fiducial points are effectively the peaks of, respectively, the highest and lowest clearly visible pulse components), and *ii*) the angular separation between the left-most peak and the “precursor” visible on some days 0.3 in pulse phase preceding it (which is generally much fainter than the main components, but not always: see, e.g., the profiles for MJDs 53913 and 53951) also remains constant within the uncertainties. Also commending this method is the empirical consideration that it works well, with only a handful of TOAs rejected because their pre-fit residuals are particularly large, owing presumably to “awkward” pulse shapes. The TOAs thus obtained for timing purposes (§ 2.2) also match (up to a constant offset of ≈ 25 ms) those obtained via the standard cross-correlation method for data acquired before mid-July (when profile variation is the smallest).

2.1.2. Parkes

The first detection of radio pulsations from XTE J1810–197 took place at the ATNF Parkes telescope on 2006 March 17, with confirmation following on April 25 (Camilo et al. 2006). Since then we have observed the pulsar there at frequencies

ranging from 0.7 to 8.4 GHz using a variety of spectrometers. Unless otherwise noted, in this paper we use only 1.4 GHz data, obtained with the analog filterbanks as described by Camilo et al. (2006).

The 1.4 GHz Parkes data set is very sparse by comparison with Nançay’s, but is particularly useful here for two purposes: to extend the overall timing span by more than one month, and to perform consistency checks on the timing solution using two independent sets of TOAs. Because the vast majority of the Parkes data used here were obtained before late July (when pulse shapes were relatively stable; see Fig. 1 and § 2.1.1), the standard cross-correlation method that we used to obtain these TOAs works well enough.

2.1.3. GBT

We have observed XTE J1810–197 at the NRAO Green Bank Telescope (GBT) since 2006 May 2 at frequencies spanning 0.3–42 GHz. Very few of these data are at 1.4 GHz and, unless noted otherwise, no GBT data were used here for timing purposes. Instead, using its large gain, bandwidth, and frequency agility, we have obtained very high-quality pulse profiles at a number of widely-separated frequencies that illustrate the remarkable time-variation in pulse shapes displayed by this magnetar. Some examples of this collection at a frequency of 1.9 GHz are shown in Figure 2.

2.1.4. VLA

We have used a sub-array of the NRAO Very Large Array (VLA) to measure with high precision the flux density of XTE J1810–197 at 1.4 GHz on 13 days between 2006 February 28 and September 5. During a typical observation we accumulate 40 min of on-source visibilities in continuum mode, with a bandwidth of 100 MHz. Each observation begins with a ≈ 5 min scan of a flux calibrator, either 3C286 or 3C48. The remainder of the observation consists of three ≈ 2 min scans of the phase calibrator 1811–209 interspersed with two ≈ 20 min on-source scans. The recorded visibilities are calibrated and imaged using standard procedures in the Astronomical Image Processing System. Due to variations in the array configuration, the number of antennas used, and the amount of observing time allocated, the errors in our flux density measurements range between 0.2 mJy and 1.0 mJy.

2.1.5. Chandra

XTE J1810–197 was observed with the *Chandra X-ray Observatory* on 2006 September 10–11, using the back-illuminated S3 chip of the ACIS-S CCD detector in TIMED/VFAINT mode with a sub-array readout that provided a time resolution of 0.441 s, and deadtime of 9%. Data were acquired continuously over an interval of 8.4 hr starting at 19:40 UT with no background contamination. All photon arrival times were corrected to the solar system barycenter (TDB) using the JPL DE200 ephemeris and the *axbary* task in the Chandra Interactive Analysis of Observations. Photons falling within an aperture of radius $3''$ centered on XTE J1810–197 were extracted from the standard processing event Level 2 data files and a total of 7014 counts were accumulated in the 0.5–3.0 keV energy range, chosen to maximize the source signal-to-noise ratio.

The barycentered photon arrival times were folded at epoch MJD 53989.0 (midnight TDB on September 11) into 10 bins using $P = 5.540362$ s determined from a simultaneous radio observation at the GBT (see § 2.2.1).

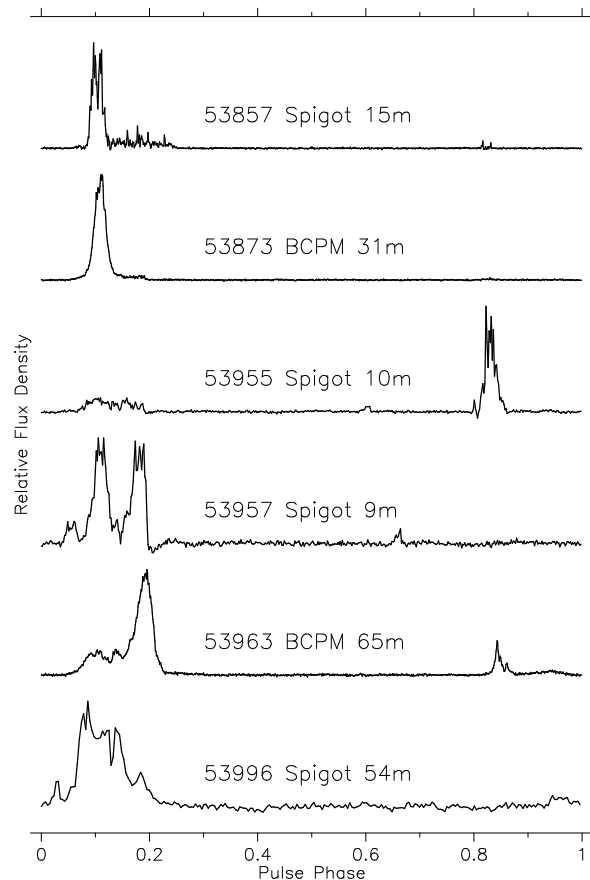


FIG. 2.— Changing pulse shapes of XTE J1810–197 from GBT observations. All profiles were aligned with the polynomial used for Figure 1. The labels list the observation date (MJD), spectrometer used, and effective integration time in minutes. Spigot (Kaplan et al. 2005) data were recorded across a 600 MHz band centered at 1.95 GHz, while a 134 MHz band centered on 1.85 GHz was used for BCPM (Backer et al. 1997). Note the low-level emission near phases 0.8 on MJDs 53857, 0.6 on 53955, 0.65 on 53957, and 0.95 on 53963. See also Figure 5.

2.2. Timing

We have used the available TOAs (§§ 2.1.1 and 2.1.2), along with the TEMPO⁷ software, to obtain the timing solution that describes the rotational history of XTE J1810–197 during 2006 May–October. Because of the changing pulse shapes and heterogeneity of the available data (§ 2.1), particular care must be taken with this process.

First we used Nançay TOAs to obtain a solution spanning June–October. Starting with a handful of TOAs and an initial solution fitting only for rotational phase and frequency $\nu = 1/P$, we subsequently added $\dot{\nu}$ as needed. We then added one TOA at a time, paying particular attention to its pre-fit residual and corresponding pulse shape, as well as the post-fit residuals and fit parameters. In this way we eliminated seven TOAs, from a set of 100, that had large ($\gtrsim 100$ ms) pre-fit residuals; these could usually be ascribed to particularly unusual pulse shapes. After approximately one month it is no longer possible to obtain featureless timing residuals without fitting for higher frequency derivatives. After this we added the Parkes TOAs, fitting also for an offset between both TOA sets to account for an arbitrary alignment between the respective fiducial points. The magnitude of this offset (21 ± 15 ms; unless otherwise stated, the uncertainties used in this paper

⁷ See <http://www.atnf.csiro.au/research/pulsar/tempo/>

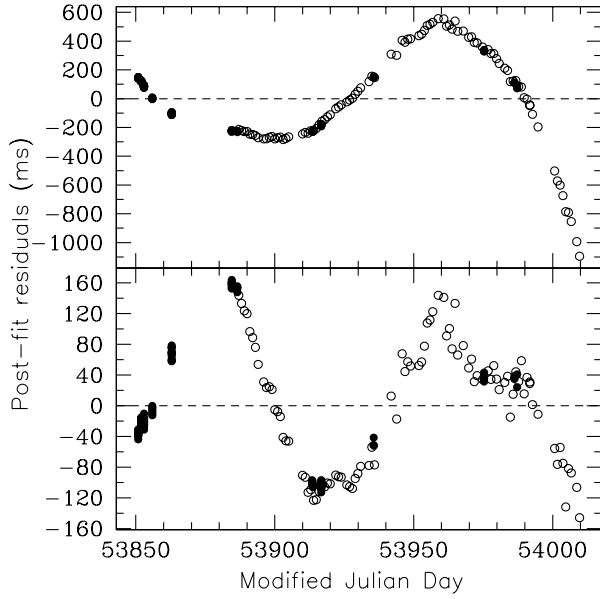


FIG. 3.— Timing residuals for XTE J1810-197. *Open circles* correspond to Nançay TOAs, while *filled circles* represent Parkes TOAs (see § 2.1). *Top panel:* Residuals for a model that contains only the rotation phase, frequency ν and $\dot{\nu}$ (see Table 1), showing a clear cubic residual trend. *Bottom panel:* Residuals for a model with an additional polynomial term, $\ddot{\nu} = 5.8 \pm 0.1 \times 10^{-21} \text{ s}^{-3}$. Note the change in vertical scale by a factor of five, and the remaining quartic trend.

all represent 1σ confidence levels) is as expected, considering the different methods used to obtain the respective TOAs (see §§ 2.1.1 and 2.1.2).

In general it is difficult to estimate TOA uncertainties reliably for our data, owing to changing pulse shapes and the principal method used to obtain TOAs (see § 2.1.1). For the early Parkes data these are typically in the 5–10 ms range. The uncertainty of early Nançay TOAs is more often 10–20 ms. Following the general weakening of the pulsar, the broadening of its profile components, and the huge variability displayed by the pulse shapes (Fig. 1), we estimate that the TOA uncertainties are commonly around 25–50 ms but can reach values approaching 100 ms on occasion. As noted above we have excluded from the timing fits a few TOAs with such large pre-fit residuals (and estimated uncertainties). Because of these difficulties, we assigned a uniform weight to the TOAs, and as a result we do not obtain a χ^2 figure of merit for the timing fits. Nevertheless, the TOA uncertainty estimates noted here are in keeping with the corresponding fit rms residuals.

We obtained a phase-connected timing solution that encompasses all data beginning with the confirmation TOAs from April 25 (we comment below on use of the discovery TOAs from March 17). The residuals from a quadratic fit to pulse phase are shown in the top panel of Figure 3 and the respective solution is given in Table 1. An independent solution using only Parkes TOAs results in similar parameters. The cubic trend of large amplitude visible in the residuals points to very significant unmodeled behavior, expected of young pulsars in general, whose rotation is “noisy”, and of XTE J1810-197 in particular (Ibrahim et al. 2004). While $\dot{\nu}$ clearly varies with time, the bottom panel of Figure 3 shows that it does not do so smoothly. A total of seven frequency derivatives are required to “whiten” the residuals, which then have an rms of 16 ms.

In order to extract from this record of unsteady rotation a

TABLE 1
TIMING PARAMETERS FOR
XTE J1810-197

Parameter	Value
Right Ascension	18 ^h 09 ^m 51 ^s .087
Declination	−19°43′51″.93
DM (cm ^{−3} pc) . .	178.0
Epoch (MJD) . .	53930.0
ν (s ^{−1}) ^a	0.180495388(1)
$\dot{\nu}$ (10 ^{−13} s ^{−2}) ^a .	−2.891(4)
MJD range	53850–54009

NOTE. — The celestial coordinates were held fixed at the values obtained from VLA observations, and the DM was held fixed at the value obtained from simultaneous 0.7 and 2.9 GHz observations (see Camilo et al. 2006).

^a These two parameters are sufficient to obtain a phase-connected solution encompassing the MJD range, but do not fully describe the rotation of the neutron star. They are non-stationary and, strictly, not predictive. See Figure 3 and § 2.2 for more details.

quantitative measure of the varying torque acting on the neutron star, we have measured $\dot{\nu}$ as a function of time. We have done this in a piece-wise fashion, performing quadratic fits to phase for TOA spans long enough that the nominal resulting fractional uncertainty in $\dot{\nu}$ was no more than 3%, but short enough that no trends were seen in the residuals. In practice this implied individual segments of very nearly 30 days each. So as to better sample the variation in $\dot{\nu}$, we did this with Nançay data while stepping through the TOAs in offsets of 15 days. A fit to all the good Nançay TOAs using seven frequency derivatives also yields $\dot{\nu}(t)$, although without associated uncertainties.

Owing to the lack of Nançay observations and the sparser data from Parkes and GBT, this was not straightforward before June 1. We opted for performing timing fits using multi-frequency data from both Parkes and GBT, thereby gaining some additional leverage in our solutions. At this time, the radio emission at most frequencies was usually dominated by a single narrow component (see Camilo et al. 2006), so that TOA artifacts were relatively small. In this manner we obtained a $\dot{\nu}$ measurement for late April–late May. Finally, we also used the March 17 Parkes discovery observations in a timing fit. We appear to have maintained phase connection with the confirmation observations 39 days later (the pre-fit residual between the discovery TOAs and the solution computed with the first month of data following confirmation is only 0.16P). However we have established with Nançay data that cubic trends typically become significant for $\gtrsim 30$ days, and we have therefore obtained this earliest measurement of $\dot{\nu}$ also by computing the difference in barycentric frequencies between March 17 and April 25. The two $\dot{\nu}$ values differ by only 2.7σ of the (much smaller) uncertainty of the phase-connected fit, and this agreement allows us to extend our record of $\dot{\nu}$ by one additional month.

The run of $\dot{\nu}$ measured over 6.5 months is shown in the top panel of Figure 4. The overall trend is one of increasing $\dot{\nu}$, as could be inferred from the top panel of Figure 3, but the way in which this occurs appears remarkable. In the three months prior to mid-July, $\dot{\nu}$ varied in relatively steady fash-

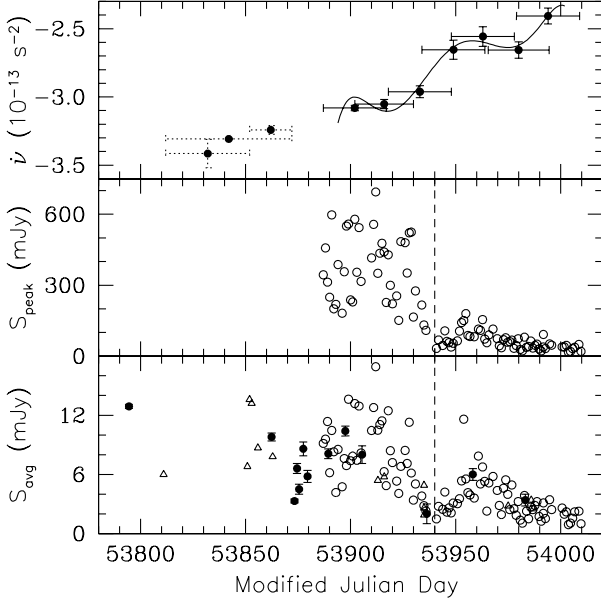


FIG. 4.— Frequency derivative and flux densities at 1.4 GHz for XTE J1810–197. *Top panel:* Frequency derivative obtained for a variety of timing fits each spanning about 30 days. *Solid error bars* denote fits obtained with Nançay data alone, while *dotted error bars* correspond to fits that contain Parkes and in some cases also GBT data. For Nançay fits the error bars represent nominal 2σ confidence levels; for all others, 4σ . The *solid line* represents the model $\dot{\nu}$ from a fit to all Nançay TOAs using seven frequency derivatives. See § 2.2 for details. *Middle panel:* Daily peak flux density of the profile component used to obtain Nançay TOAs (see § 2.1.1 and Fig. 1). *Bottom panel:* Daily period-averaged flux density from Nançay (*open circles*) and Parkes (*triangles*), and continuum VLA flux density (*filled circles*; § 2.1.4).

ion, from $-3.3 \times 10^{-13} \text{ s}^{-2}$ to $-3.0 \times 10^{-13} \text{ s}^{-2}$. Then, in late July, it changed to $-2.7 \times 10^{-13} \text{ s}^{-2}$ over a span of 15 days — the implied change in torque is $-2 \times 10^{32} \text{ dyn cm}$ (using a stellar moment of inertia of 10^{45} g cm^2), which is larger than the torque powering three quarters of all known pulsars! Regardless of the detailed mechanisms that produce radio pulses in XTE J1810–197, it should perhaps not be surprising if other observational properties of the magnetar should have changed around this time.

In fact, as the middle panel of Figure 4 shows, the peak flux density of XTE J1810–197 has dramatically decreased since about that time. Interestingly, while the period-averaged flux density has also decreased compared to its average value before mid-July (bottom panel of Fig. 4), it has done so by a smaller factor and continues to fluctuate greatly from day to day (when such values are available from two of Nançay, Parkes or VLA within a day of each other, they are consistent within expectations given the inherent variations). These two observations can be understood by inspection of the profiles shown in Figure 1: since late July, the daily profiles of XTE J1810–197 have tended to be composed of two (or more) significant peaks, each much broader than the one peak generally prominent before that time (with typical full-width at half-maximum $\approx 0.04P$, versus about half that value beforehand), and the pulse-shape variance is greater than before. This may also explain why the Nançay timing residuals for each one-month fit after mid-July are about 24 ms rms, twice as large as the typical corresponding value before then.

2.2.1. X-ray and radio pulse alignment

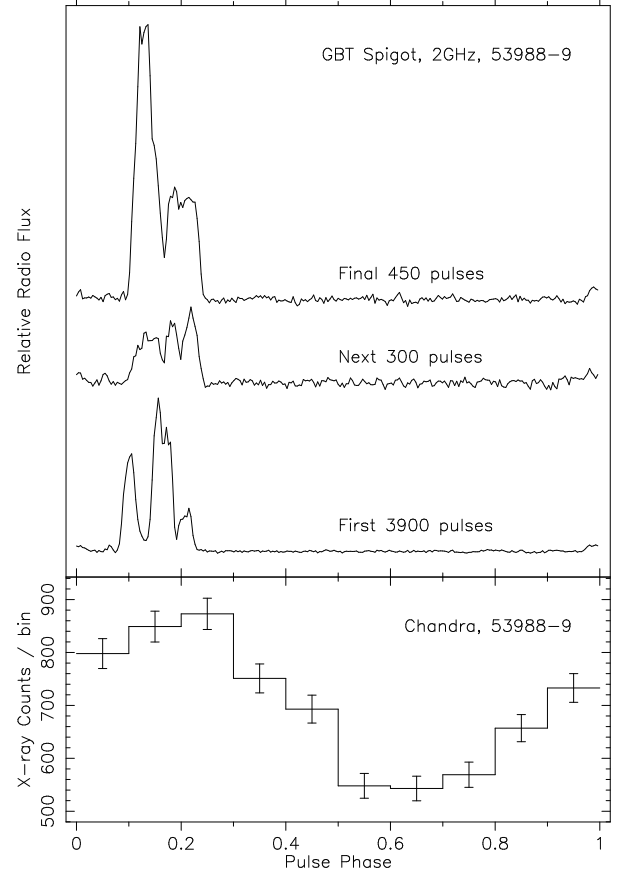


FIG. 5.— *Bottom panel:* X-ray pulse profile (0.5–3.0 keV) of XTE J1810–197 from an observation with *Chandra* on 2006 September 10–11, folded with barycentric $P = 5.540362 \text{ s}$ as determined from a simultaneous radio observation (see § 2.1.5). Phase zero on this plot corresponds to MJD 53989.0 (TDB). *Top panel:* Radio profiles from a simultaneous GBT observation, starting on September 10, 20:50 UT. After 6 hr (*bottom trace*), the pulse profile abruptly changed to a different configuration for 30 min (*middle trace*), after which it changed yet again (*top trace*). The relative integrated flux densities of the three profiles are 1.4, 1.0, 2.9, from bottom to top. The middle peak of the bottom radio profile arrives at phase 0.17 on the plot, and all four profiles are absolutely aligned (see § 2.2.1). Note also the alignment between the left-most peak of the top profile and the first notch in the bottom profile.

On 2006 September 10–11 we observed XTE J1810–197 for 7.2 hr with the GBT at 1.9 GHz, starting 1 hr after the beginning of the *Chandra* observation (§ 2.1.5). We have used the contemporaneous TOAs thus obtained to measure the phase offset between the X-ray and radio pulses. The folded X-ray profile is shown in Figure 5, with the first phase bin chosen to begin at midnight on September 11 (TDB). After translating the TOAs for the first radio profile (see Fig. 5) converted to infinite frequency to the solar system barycenter, a TEMPO fit yields a phase offset for the fiducial point of the radio profile (here its middle peak) of 0.167 ± 0.006 in the Figure. The uncertainty includes a component due to the fit and a slightly smaller contribution from the uncertainty in the dispersion measure (DM) of XTE J1810–197.

Within the larger uncertainty imposed by the *Chandra* resolution ($0.08P$; see § 2.1.5) and the relatively small number of pulsed X-ray counts, the main component of the radio profile on this day arrives at the same time as the peak of the X-ray pulse (Fig. 5).

Interestingly, the radio profile changed in both shape and flux during the *Chandra* observation — twice, within a span of 30 min (Fig. 5). This does not modify the conclusion in

the above paragraph, but helps answer a question concerning the radio flux and profile variations observed in XTE J1810–197: they can occur suddenly (observed at a resolution of ~ 10 s). We have “caught in the act” at least four such changes at Nançay and one each at the GBT and Parkes, all since mid-July. As this corresponds to some 100 hours of observing time, we can estimate that such transitions occur on average every ~ 15 hr, at the present epoch. No X-ray bursts or significant changes in the X-ray flux or pulse shape were seen at the times of the radio transitions indicated in Figure 5. The *Chandra* count rates during the three radio pulse states — 0.235 ± 0.003 , 0.213 ± 0.011 , and $0.218 \pm 0.007 \text{ s}^{-1}$, respectively — are uncorrelated with the large changes in radio flux density and pulse shapes.

3. DISCUSSION

All young radio pulsars experience rotational instabilities, observed as a continuous quasi-stochastic wandering of the pulse phase (“timing noise”) or discontinuous spin-up events (“glitches”). These are thought ultimately to be driven by the unsteady transfer of angular momentum from the interior superfluid to the crust of the neutron star. XTE J1810–197 displays large amounts of timing noise-like behavior; despite very large changes observed in $\dot{\nu}$ on short time scales, all observed rotational changes have been continuous to within the available resolution and we have not observed any glitch-like behavior. Arzoumanian et al. (1994) quantified timing noise as the time-magnitude of its cumulative contribution over a time interval t to the cubic term in a Taylor series expansion of rotational phase, i.e., $\ddot{\nu}t^3/(6\nu)$. For XTE J1810–197 this amounts to 14 s over 160 days, a huge amount that far surpasses anything observed in radio pulsars and is also greater than an extrapolation based on the notion that the magnitude of timing noise is proportional to \dot{P} (Arzoumanian et al. 1994). However, this level of timing noise is not unprecedented for magnetars.

Six AXPs, including XTE J1810–197, and two soft-gamma repeaters (SGRs), i.e., the majority of all known magnetars, have been observed with phase connection maintained for at least a few months (see Woods & Thompson 2006, and references therein). The SGRs 1806–20 and 1900+14 usually have the largest amounts of timing noise, approximately two orders of magnitude above the level we observe in XTE J1810–197, with $\dot{\nu}$ varying by factors of two within 1 yr, and four overall (Woods et al. 2002). The rotational stability of AXPs is generally greater (although two have been observed to glitch), and four are substantially quieter than XTE J1810–197. The remaining one, 1E 1048.1–5937, has been relatively quiet in the last two years (Kaspi 2006), but previously displayed far greater rotational instability than observed in XTE J1810–197 (Gavril & Kaspi 2004). Therefore, while noisier than most AXPs, XTE J1810–197 may not be particularly remarkable in this respect. What is unusual is that we can now track its rotation via daily observations, in greater detail than is possible for other AXPs.

Following its discovery with the *Rossi X-ray Timing Explorer*, a phase-connected solution was obtained for XTE J1810–197 spanning 2003 January–September, during which $\dot{\nu}$ varied between $-6.7 \times 10^{-13} \text{ s}^{-2}$, averaged over eight months, and $-3.8 \times 10^{-13} \text{ s}^{-2}$ over the last two months (Ibrahim et al. 2004). The very large initial magnitude may have reflected in part transients associated with a putative glitch at the time of the X-ray outburst in early 2003. In the succeeding 2.5 years phase connection was no longer possi-

ble owing to the sparse sampling, but individual period measurements six months apart established that the average $\dot{\nu}$ was $-2.5 \times 10^{-13} \text{ s}^{-2}$ between late 2003 and early 2004 (see Gotthelf & Halpern 2005). The range of $\dot{\nu}$ that we have measured over six months in 2006 therefore falls within the historical range for this source, which can be summarized as $\dot{\nu} = (-3.1 \pm 0.7) \times 10^{-13} \text{ s}^{-2}$ over the past three years. Importantly, although $\dot{\nu}$ has increased almost monotonically during our radio observations (Fig. 4), it cannot have been increasing during the entirety of the past three years (see also Gotthelf & Halpern 2006). Periods of decreasing torque such as we have observed recently must have been interspersed with at least one epoch of substantially increasing torque.

In ordinary pulsars, the observed rotational instabilities are mainly presumed to be caused by angular momentum transfer processes internal to the neutron star. In the magnetar model, the external energy stored in the magnetosphere, partly released through reconfiguration and decay of the magnetic field and currents, may also lead to erratic variations in the torque acting upon the star, for example via a flux of Alfvén waves and particles resulting from magnetically-induced (sudden large-scale or persistent small-scale) crustal seismic activity (e.g., Thompson et al. 2000). It is unclear whether any such particular models (see also Duncan 2001) can explain the magnitude and time scale of the variations in torque currently observed in XTE J1810–197, nearly four years after the X-ray outburst. In any case, substantial variations in magnetospheric plasma densities and/or currents would likely have implications for other observable properties of the pulsar.

An interesting comparison is with PSR B1931+24, an ordinary radio pulsar during intervals of 5–10 days, with $P = 0.8$ s and $B \approx 2 \times 10^{12}$ G, which abruptly shuts off for 25–35 days in a pattern that repeats quasi-periodically (Kramer et al. 2006). During these turned-off periods, the torque is only two thirds of its turned-on value. Kramer et al. (2006) conclude from this extraordinary behavior that the occasional presence of a plasma leads to radio emission and its flow provides the extra braking torque. The plasma density calculated from the torque difference is 100 esu cm^{-3} , in agreement with the corotation value (Goldreich & Julian 1969). In XTE J1810–197 the radio emission has not shut off, but it did diminish and change markedly in character somewhat abruptly in late July, apparently coincident with a huge reduction in torque ($\dot{\nu}$ changed from $-2.96 \times 10^{-13} \text{ s}^{-2}$ on MJD 53933 to $-2.65 \times 10^{-13} \text{ s}^{-2}$ on MJD 53949; see § 2.2 and Fig. 4). A calculation such as that by Kramer et al. (2006) would suggest for XTE J1810–197 an “extra” plasma density of about 300 esu cm^{-3} prior to the large torque decrease, compared to the source’s Goldreich-Julian density of 1350 esu cm^{-3} . Implicit in this calculation is the notion that the radio emission originates from open field lines, which has not been proven for XTE J1810–197. However, the pulse profile and flux variations observed in XTE J1810–197 occur on time scales that are apparently too short to be explained by changes in the closed field lines (see, e.g., Beloborodov & Thompson 2006).

If indeed the measured changes in torque are caused by variations in the magnetospheric plasma density in locations relevant for the production of coherent radio emission, then it should be no surprise that the pulse profiles of XTE J1810–197 change so remarkably: even the “small” torque changes reflected in Figure 4 are enormous by the standards of ordinary pulsars. And certainly, the profile variations in XTE J1810–197 (Figs. 1, 2 and 5) are observationally distinct from the “mode changing” of some ordinary pulsars,

where the average pulse profile suddenly changes between two of a small set of different configurations (e.g., Bartel et al. 1982); XTE J1810–197 displays a much greater variety. However, the root cause of mode changing is not well understood, and we have established that XTE J1810–197 profiles can change suddenly (Fig. 5), so that some link may exist between these two phenomena. Other behavior, like the broader pulse components typically observed after MJD 53940, even as the phase separation between components remains largely fixed (Fig. 1 and § 2.2), also appears extraordinary.

Compared to such extreme radio variability, the X-ray spectrum and pulse profiles of XTE J1810–197 change slowly as the flux decays (e.g., Gotthelf & Halpern 2006), on a much longer time scale (~ 1 yr) than the fluctuations in torque reported here. The alignment of the peaks of the radio and X-ray pulses suggests that the footpoints of the active magnetic field lines on which radio emission is generated are also the locations of concentrated crustal heating that is responsible for the enhanced X-ray emission, at least at the higher energies that apparently come from a relatively small area (see Gotthelf & Halpern 2006). However, even if the energetic particle bombardment that heats the surface hot spot fluctuates on time scales of less than one day, the absence of correlated X-ray variability on similar time scales indicates that most of the X-ray luminosity originated in deeper crustal heating at the time of the X-ray turn on, or from more gradual decay of the magnetic field (Eichler & Cheng 1989).

Some persistent AXPs have shown substantial variability in X-ray flux (e.g., Gavriil & Kaspi 2004), quite apart from the phenomenon of X-ray bursts (for bursts in XTE J1810–197, see Woods et al. 2005); their pulse profiles generally appear to be fairly stable (Gavriil & Kaspi 2002), although they can change following glitches (e.g., Kaspi et al. 2003). In any case, despite often great fluctuations in torque, there is no

confirmed correlation between observed variations in radiative properties and the detailed rotational evolution of persistent AXPs (1E 1048.1–5937 is a possible counter-example; Gavriil & Kaspi 2004).

With observations of XTE J1810–197, we now find ourselves in the curious position of relying upon energetically insignificant radio pulsations exhibiting a remarkably diverse phenomenology to illuminate rather more energetic events on the magnetar. Attempting to understand key aspects of the radio observations may perhaps lead to a deeper understanding of both magnetars and radio pulsar emission.

We are grateful to John Sarkissian for help with Parkes observations, Eric Gerard for useful discussions concerning Nançay flux calibration, and David Nice for wisdom on time systems as used in TEMPO. The Nançay radio telescope is part of the Paris Observatory, associated with the Centre National de la Recherche Scientifique (CNRS), and partially supported by the Region Centre in France. The National Radio Astronomy Observatory is a facility of the National Science Foundation, operated under cooperative agreement by Associated Universities, Inc. The Parkes Observatory is part of the Australia Telescope, which is funded by the Commonwealth of Australia for operation as a National Facility managed by CSIRO. FC thanks the NSF for support through grant AST-05-07376. EVG acknowledges support for this work provided by the National Aeronautics and Space Administration through Chandra Award Number GO6-7044X issued by the Chandra X-ray Observatory Center, which is operated by the Smithsonian Astrophysical Observatory for and on behalf of NASA under contract NAS8-03060; and by NASA ADP grant NNG05GC43G.

REFERENCES

- Arzoumanian, Z., Nice, D. J., Taylor, J. H., & Thorsett, S. E. 1994, *ApJ*, 422, 671
- Backer, D. C., Dexter, M. R., Zepka, A., D., N., Wertheimer, D. J., Ray, P. S., & Foster, R. S. 1997, *PASP*, 109, 61
- Bartel, N., Morris, D., Sieber, W., & Hankins, T. H. 1982, *ApJ*, 258, 776
- Beloborodov, A. M., & Thompson, C. 2006, *ApJ*, in press (astro-ph/0602417)
- Camilo, F., Ransom, S. M., Halpern, J. P., Reynolds, J., Helfand, D. J., Zimmerman, N., & Sarkissian, J. 2006, *Nature*, 442, 892
- Cognard, I., & Theureau, G. 2006, On the Present and Future of Pulsar Astronomy, 26th meeting of the IAU, JD02, #36, 2
- Duncan, R. C. 2001, in *AIP Conf. Proc. 556: Explosive Phenomena in Astrophysical Compact Objects*, ed. H.-Y. Chang, C.-H. Lee, M. Rho, & I. Yi, 228
- Eichler, D., & Cheng, A. F. 1989, *ApJ*, 336, 360
- Gavriil, F. P., & Kaspi, V. M. 2002, *ApJ*, 567, 1067
- . 2004, *ApJ*, 609, L67
- Goldreich, P., & Julian, W. H. 1969, *ApJ*, 157, 869
- Gotthelf, E. V., & Halpern, J. P. 2005, *ApJ*, 632, 1075
- Gotthelf, E. V., & Halpern, J. P. 2006, in *Isolated Neutron Stars: From the Interior to the Surface*, ed. S. Zane, R. Turolla, & D. Page, in press (astro-ph/0608473)
- Halpern, J. P., & Gotthelf, E. V. 2005, *ApJ*, 618, 874
- Halpern, J. P., Gotthelf, E. V., Becker, R. H., Helfand, D. J., & White, R. L. 2005, *ApJ*, 632, L29
- Ibrahim, A. I., et al. 2004, *ApJ*, 609, L21
- Kaplan, D. L., Escoffier, R. P., Lacasse, R. J., O’Neil, K., Ford, J. M., Ransom, S. M., Anderson, S. B., Cordes, J. M., Lazio, T. J. W., & Kulkarni, S. R. 2005, *PASP*, 117, 643
- Kaspi, V. M. 2006, in *Isolated Neutron Stars: From the Interior to the Surface*, ed. S. Zane, R. Turolla, & D. Page, in press (astro-ph/0610304)
- Kaspi, V. M., Gavriil, F. P., Woods, P. M., Jensen, J. B., Roberts, M. S. E., & Chakrabarty, D. 2003, *ApJ*, 588, L93
- Kramer, M., Lyne, A. G., O’Brien, J. T., Jordan, C. A., & Lorimer, D. R. 2006, *Science*, 312, 549
- Thompson, C., Duncan, R. C., Woods, P. M., Kouveliotou, C., Finger, M. H., & van Paradijs, J. 2000, *ApJ*, 543, 340
- Woods, P. M., Kouveliotou, C., Göğüş, E., Finger, M. H., Swank, J., Markwardt, C. B., Hurley, K., & van der Klis, M. 2002, *ApJ*, 576, 381
- Woods, P. M., Kouveliotou, C., Gavriil, F. P., Kaspi, V. M., Roberts, M. S. E., Ibrahim, A., Markwardt, C. B., Swank, J. H., & Finger, M. H. 2005, *ApJ*, 629, 985
- Woods, P. M., & Thompson, C. 2006, in *Compact Stellar X-ray Sources*, ed. W. H. G. Lewin & M. van der Klis (Cambridge: CUP), in press (astro-ph/0406133)